Oxidation of Metal–*meso*-Octaethylporphyrinogen Complexes Leading to Novel Oxidized Forms of Porphyrinogen Other than Porphyrins. 2. The Redox Chemistry of Iron(II)- and Cobalt(II)–*meso*-Octaethylporphyrinogen Complexes Occurring with the Formation and Cleavage of Two Cyclopropane Units

Stefania De Angelis,† Euro Solari,† Carlo Floriani,*,† Angiola Chiesi-Villa,‡ and Corrado Rizzoli‡

Contribution from the Institut de Chimie Minérale et Analytique, Université de Lausanne, Place du Château 3, CH-1005 Lausanne, Switzerland, and Istituto di Strutturistica Chimica, Centro di Studio per la Strutturistica Diffrattometrica del CNR, Università di Parma, I-43100 Parma, Italy

Received January 20, 1994®

Abstract: In this paper we report a four-electron oxidation of a porphyrinogen tetraanion leading to a neutral form containing two cyclopropane units complexes to iron(II), iron(III), and cobalt(II). The redox chemistry of the *meso*-octaethylporphyrinogen–cobalt(II) complex clarified the stepwise process leading to the oxidized forms of porphyrinogen. The reaction of the iron(II)–*meso*-octaethylporphyrinogen complex $[Et_8N_4FeLi_2(THF)_4]$ (**1**) with $CuCl_2$ led to a four-electron oxidation of the porphyrinogen skeleton and the formation of two cyclopropane units. Such an oxidation converts the *meso*-octaethylporphyrinogen tetraanion into a neutral ligand which is bonded *via* the nitrogen atoms to the $[FeCl]^+$ cation and with a C=C double bond of each pyrrole to the four copper(I) atoms of the $[Cu_4Cl_5]^-$ cluster in $[Et_8N_4(\Delta)_2FeCl\cdots Cu_4Cl_5]$ (**2**). The stabilization of the four-electron oxidized form is independent of interaction with the $[Cu_4Cl_5]^-$ cluster, as proven by the isolation of a copper free form. The oxidation of $[Et_8N_4]^-[Li(THF)_4]^+$ (**3**) with $CuCl_2$ under different conditions led to the porphyrinogen–bis(cyclopropane) form binding exclusively iron(III) in $[Et_8N_4(\Delta)_2FeCl]^{2+}[FeCl_4]^{2-}$ (**4**) [(Δ) = abbreviation for cyclopropane]. The structure of **4** has been established by an X-ray analysis. A comparison between the structures of **1** and **4** singles out the conformational changes occurring on the porphyrinogen skeleton upon a four-electron oxidation and formation of two cyclopropane units. The stepwise nature of such an oxidation has been clarified by studying the oxidation of $[Et_8N_4CoLi_2(THF)_4]$ (**5**), which can be converted by reaction with 1 mol of $CuCl_2$ to the corresponding cobalt(III) derivative $\{[Et_8N_4Co]^-[Li(THF)_4]^+\}$ (**6**) and undergoes a further oxidation by $CuCl_2$ to $[Et_8N_4(\Delta)Co]$ (**7**), containing the oxidized form of porphyrinogen with a cyclopropane unit. An intermolecular redox process, dependent on the nature of the solvent, occurs between **7** and **5**, leading to the formation of **6**. In the presence of coordinating solvents, **6** is the stable form, while in hydrocarbons, it disproportionates into **5** and **7**. The best synthesis of **7** is achieved by the oxidation of **5** with an excess of *p*-benzoquinone. The cyclopropane unit can be reduced by two electrons by reacting **7** with excess lithium metal or by reductive demetalation with H_2S. The reaction of **7** with $CuCl_2$ leads to a further oxidation of porphyrinogen by two electrons and the formation of a second cyclopropane unit. The fully oxidized form of porphyrinogen is a neutral ligand. Complex **8**, $[\{Et_8N_4(\Delta)_2CoCl\}\cdots\{Cu_4Cl_5\}]$, has been structurally characterized and like **2** contains the oxidized form bonded to $[CoCl]^+$ *via* nitrogen atoms and to the $[Cu_4Cl_5]^-$ cluster *via* the pyrrolic C=C bonds. Crystallographic details: **1** is monoclinic, space group $C2/c$, $a = 20.749(2)$ Å, $b = 10.930(1)$ Å, $c = 22.797(2)$ Å, $\alpha = \gamma = 90°$, $\beta = 104.69(2)°$, $Z = 4$, and $R = 0.044$. **4** is orthorhombic, space group $Pbca$, $a = 23.144(4)$ Å, $b = 30.264(7)$ Å, $c = 13.362(3)$ Å, $\alpha = \beta = \gamma = 90°$, $Z = 8$, and $R = 0.053$. **7** is monoclinic, space group $P2_1$, $a = 15.804(2)$ Å, $b = 12.237(1)$ Å, $c = 17.026(3)$ Å, $\alpha = \gamma = 90°$, $\beta = 91.15(2)°$, $Z = 4$, and $R = 0.069$. **8** is triclinic, space group $P\bar{1}$, $a = 15.361(3)$ Å, $b = 15.548(4)$ Å, $c = 12.060(5)$ Å, $\alpha = 107.66(2)°$, $\beta = 99.62(2)°$, $\gamma = 86.30(2)°$, $Z = 2$, and $R = 0.080$.

Introduction

Although *meso*-octaalkylporphyrinogens, a class of molecules whose prototype was discovered by Baeyer in 1886,[1] have some unique chemical and topological properties, they have not received much attention.[2] One of the most interesting aspects of *meso*-octaalkylporphyrinogen chemistry is related to its use as a ligand for transition metals, a field entered by this group in recent years.[3-8]

The tetraanion generated by reaction of the *meso*-octaethyl derivative $Et_8N_4H_4$[3] with Bu^nLi gave rise to a starting material, $[Et_8N_4Li_4(THF)_4]$,[5] which allowed entry into organometallic and coordination chemistry in nonaqueous solutions.

* To whom correspondence should be addressed.
† Université de Lausanne.
‡ Università di Parma.
® Abstract published in *Advance ACS Abstracts*, June 1, 1994.

(1) Baeyer, A. *Chem. Ber.* **1886**, *19*, 2184.
(2) (a) Fischer, H.; Orth, H. *Die Chemie des Pyrrols*; Akademische Verlagsgesellschaft; Leipzig, Germany, 1934; p 20. (b) Dennstedt, M.; Zimmermann, J. *Chem. Ber.* **1887**, *20*, 850, 2449; **1888**, *21*, 1478. (c) Dennstedt, D. *Chem. Ber.* **1890**, *23*, 1370. (d) Chelintzev, V. V.; Tronov, B. V. *J. Russ. Phys.-Chem. Soc.* **1916**, *48*, 105, 127. (e) Sabalitschka, Th.; Haase, H.; *Arch. Pharm.* **1928**, *226*, 484. (f) Rothemund, P.; Gage, C. L. *J. Am. Chem. Soc.* **1955**, *77*, 3340.
(3) Jacoby, D.; Floriani, C.; Chiesi-Villa, A.; Rizzoli, C. *J. Chem. Soc., Chem. Commun.* **1991**, 220.
(4) Jacoby, D.; Floriani, C.; Chiesi-Villa, A.; Rizzoli, C. *J. Chem. Soc., Chem. Commun.* **1991**, 790.
(5) Jacoby, D.; Floriani, C.; Chiesi-Villa, A.; Rizzoli, C. *J. Am. Chem. Soc.* **1993**, *115*, 3595.
(6) Jubb, J.; Jacoby, D.; Floriani, C.; Chiesi-Villa, A.; Rizzoli, C. *Inorg. Chem.* **1992**, *31*, 1306.
(7) Jacoby, D.; Floriani, C.; Chiesi-Villa, A.; Rizzoli, C. *J. Am. Chem. Soc.* **1993**, *115*, 7025.
(8) Jubb, J.; Floriani, C.; Chiesi-Villa, A.; Rizzoli, C. *J. Am. Chem. Soc.* **1992**, *114*, 6571.

0002-7863/94/1516-5702$04.50/0

Scheme 1

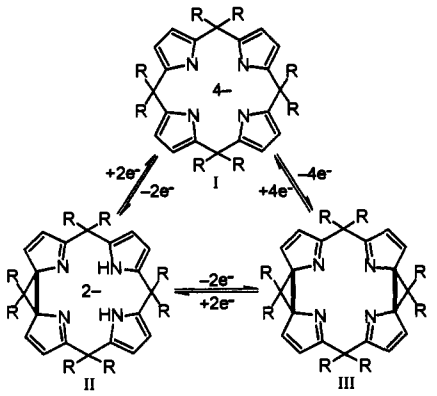

Some of the most peculiar properties of the porphyrinogen skeleton are the following: (i) The three-dimensional properties derived from the presence in the *meso*-position of sp^3 carbon allow different conformations and cavity effects[3-6] resembling those of a calix[4]arene.[9] (ii) The four pyrrolyl anions, as a consequence of the conformational flexibility, can display η^5-, η^3-, and η^1-bonding modes with the central metal ion.[4,5,7] (iii) The *meso*-alkyl groups closely approach the metal center in a manner appropriate for a subsequent C–H bond activation.[3,5,6] (iv) The electron-rich periphery, in addition to the N_4 cavity, functions as a binding site for cationic species.[5-7] (v) Its oxidation, unlike the aromatization to the porphyrin skeleton, gives rise to novel forms of oxidized porphyrinogen.[8,10]

The three former aspects are particularly important for establishing a novel organometallic chemistry based on the porphyrinogen skeleton, while the last two allowed the discovery of novel metal-assisted redox chemistry of the porphyrinogen ligand, which is the subject of this and the previous paper.[10]

The oxidation of *meso*-octaalkylporphyrinogen has two relevant aspects: (i) the possible understanding of an alternative mechanism for the oxidation of normal porphyrinogen to porphyrins[10-14] containing four hydrogen atoms in the *meso*-positions, and (ii) the generation and chemical use of oxidized forms of porphyrinogen. The oxidized forms of *meso*-octaalkylporphyrinogen can have a relevant role in ligand–, metal–, or metal–ligand based redox processes. The oxidation of a *meso*-octaalkylporphyrinogen was achieved when the tetraanion (I) was bonded to a transition metal, and its redox chemistry can be envisaged to occur as shown in Scheme 1. The oxidized forms II and III contain cyclopropane units, which can be easily formed and cleaved in a two-electron exchange. The second paper of this series deals with the four-electron oxidation of porphyrinogen leading to the form III, which has been isolated and structurally characterized. This oxidation is a stepwise process which has been clarified by the isolation of a number of intermediates. The investigation has been carried out by studying the redox chemistry of *meso*-octaethylporphyrinogen–iron(II) and –cobalt(II) complexes.

Results and Discussion

In the preceeding paper[10] we analyzed the stepwise monoelectronic redox process leading to the formation (*via* a two-electron oxidation) and cleavage (two-electron reduction) of one cyclopropane unit within the porphyrinogen skeleton. Such a process, which is expected to depend on the nature of the metal, clearly never led to any further oxidation of the porphyrinogen. Here, we will examine in detail the consequences of various oxidations on iron(II)–, iron(III)–, and cobalt(II)–*meso*-octaethylporphyrinogen complexes. Unlike the corresponding Ni(II) and Cu(II) complexes, the iron(II) derivative, **1**, does not undergo a clean oxidation by molecular oxygen, quinones, or iodine, leading to identifiable compounds. The reaction of **1** with an excess of $CuCl_2$ led to the formation of crystalline solid **2**, which was isolated in a reasonable yield (reaction 1, see details in the Experimental Section).

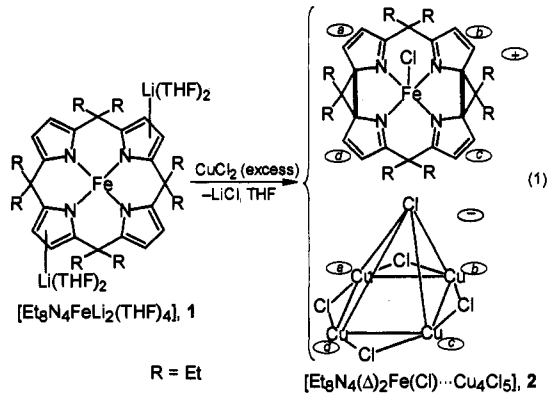

(1)

The structure of **2** was established by an X-ray analysis, although its rather low quality only allows the atom connectivity to be established and does not allow comparison of the structural parameters with those of the analogous cobalt complex, **8** (*vide infra*).

The counteranion of the iron(II) complex cation is a square pyramidal aggregate of copper(I) chloride having the framework shown in the picture. There is, however, an intimate interaction between the formal cation and anion. The four copper atoms bind to the porphyrinogen through the peripheric C=C bonds,[15] while the pyramidal Cl does not interact with the iron center (see complex **8**). The μ_{eff} at 300 K is 5.28 μ_B, which remains constant down to 20 K; this is the typical range for high-spin iron(II) complexes, and it shows a small zero field splitting.[16]

At this stage an important question may be asked: how much of the stability of the bis(cyclopropane) oxidized form is associated to its complexation to the copper(I) cluster? The isolation of an uncomplexed bis(cyclopropane)–porphyrinogen bonded to an iron(III) ion, complex **4**, clearly answers this question.

In the preceeding paper we saw how the +III oxidation state may be important as an intermediate in the oxidation of *meso*-

(9) Gutsche, C. D. *Calixarenes*; Royal Society of Chemistry: Cambridge, U.K., 1989.

(10) See the previous paper of this series (preceding article in this issue).

(11) (a) *The Porphyrins*; Dolphin, D., Ed.; Academic: New York, 1978–1979; Vols. 1–7. (b) Smith, K. M. *Porphyrins and Metalloporphyrins*; Elsevier: Amsterdam, 1975.

(12) (a) Mashiko, T.; Dolphin, D. In *Comprehensive Coordination Chemistry*; Wilkinson, G., Gillard, R. D., McCleverty, J. A., Eds.; Pergamon: Oxford, U.K., 1987; Vol. 2, Chapter 21.1, p 855. (b) Kim, J. B.; Adler, A. D.; Longo, R. F. In *The Porphyrins*; Dolphin, D., Ed.; Academic: New York, 1978; Vol. 1, Part A, p 85. Mauzerall, D. In *The Porphyrins*; Dolphin, D., Ed.; Academic: New York, 1978; Vol. 2, p 91. (c) von Maltzan, B. *Angew. Chem., Int. Ed. Engl.* **1982**, *21*, 785. (d) Lindsey, J. S.; Schreiman, I. C.; Hsu, H. C.; Kearney, P. C.; Marguerettaz, A. M. *J. Org. Chem.* **1987**, *52*, 827. Lindsey, J. S.; Wagner, R. W. *J. Org. Chem.* **1989**, *54*, 828.

(13) (a) Angst, C.; Kajiwara, M.; Zass, E.; Eschenmoser, A. *Angew, Chem., Int. Ed. Engl.* **1980**, *19*, 140. (b) Johansen, J. E.; Piermattie, V.; Angst, C.; Diener, E.; Kratky, C.; Eschenmoser, A. *Angew. Chem., Int. Ed. Engl.* **1981**, *20*, 261. (c) Franck, B. *Angew. Chem., Int. Ed. Engl.* **1982**, *21*, 343. (d) Waditschatka, R.; Diener, E.; Eschenmoser, A. *Angew. Chem., Int. Ed. Engl.* **1983**, *22*, 631. (e) Kratky, C.; Waditschatka, R.; Angst, C.; Johansen, J. E.; Plaquevent, J. C.; Schreiber, J.; Eschenmoser, A. *Helv. Chim. Acta* **1985**, *68*, 1312. (f) Waditschatka, R.; Kratky, C.; Jaun, B.; Heinzer, J.; Eschenmoser, A. *J. Chem. Soc., Chem. Commun.* **1985**, 1604.

(14) *Biosynthesis of Tetrapyrroles*; Jordan, P. M., Ed.; Elsevier: New York, 1991.

(15) For tetranuclear copper(I) complexes and their binding properties, see: Hathaway, B. J. In *Comprehensive Coordination Chemistry*; Wilkinson, G.; Gillard, R. D.; McCleverty, J. A., Eds.; Pergamon: Oxford, U.K., 1987; Vol. 5, Chapter 53.3.2.4.

(16) Casey, A. T.; Mitra, S. In *Theory and Applications of Molecular Paramagnetism*; Bodreaux, E. A., Mulay, L. N., Eds.; Wiley: New York, 1976, p 135.

Table 1. Experimental Data for the X-ray Diffraction Studies on Crystalline Compounds **1**, **4**, **7**, and **8**

compound	**1**	**4**	**7**	**8**
formula	$C_{52}H_{80}FeLi_2N_4O_4$	$C_{36}H_{48}ClFeN_4 \cdot FeCl_4 \cdot 0.5C_7H_8 \cdot 0.5C_4H_8O$	$C_{36}H_{48}CoN_4$	$C_{36}H_{48}ClCoN_4 \cdot Cu_4Cl_5 \cdot 3C_4H_8O$
a (Å)	20.749(2)	23.144(4)	15.804(2)	15.361(3)
b (Å)	10.930(1)	30.264(7)	12.237(1)	15.548(4)
c (Å)	22.797(2)	13.362(3)	17.026(3)	12.060(5)
α (deg)	90	90	90	107.66(2)
β (deg)	104.69(2)	90	91.15(2)	99.62(2)
γ (deg)	90	90	90	86.30(2)
V (Å^3)	5001.1(9)	9359.2(34)	3292.1(8)	2705.7(15)
Z	4	8	4	2
fw	895.0	907.9	595.7	1279.0
space group	$C2/c$ (no. 15)	$Pbca$ (no. 61)	$P2_1$ (no. 4)	$P\bar{1}$ (no. 2)
t (°C)	22	22	22	22
λ (Å)	0.71069	0.71069	0.71069	1.54178
ρ_{calcd} (g cm^{-3})	1.189	1.289	1.202	1.570
μ (cm^{-1})	3.48	9.40	5.47	73.24
trans coeff	0.938–1.000	0.905–1.000	0.900–1.000	0.438–1.000
R^a	0.044	0.053	0.069	0.080
$R_w{}^b$	0.043	0.053	0.074	

^{a} $R = \Sigma||\Delta F|/\Sigma|F_o|$. ^{b} $R_w = [\Sigma w^{1/2}|\Delta F|/\Sigma w^{1/2}|F_o|]$.

Table 2. Fractional Atomic Coordinates (×10^4) for Complex **1**

atom	x/a	y/b	z/c
Fe1	0(–)	2251.4(10)	2500(–)
Li1	1486(5)	3434(10)	1559(5)
O1	2253(2)	3847(5)	1255(2)
O2	866(2)	4654(4)	1154(2)
N1	849(2)	2213(4)	2296(2)
N2	458(2)	2175(4)	3347(2)
C1	971(2)	1555(4)	1820(2)
C2	1656(2)	1502(5)	1887(2)
C3	1959(2)	2181(5)	2418(2)
C4	1455(2)	2587(4)	2667(2)
C5	1480(2)	3297(5)	3241(2)
C6	1090(2)	2593(5)	3617(2)
C7	1254(2)	2290(6)	4223(2)
C8	704(3)	1636(5)	4327(2)
C9	226(2)	1590(4)	3790(2)
C10	–422(2)	864(5)	3620(2)
C11	1141(2)	4569(5)	3079(2)
C12	1485(3)	5415(5)	2726(3)
C13	2220(2)	3451(6)	3600(2)
C14	2359(3)	4354(7)	4127(3)
C15	–264(3)	–334(5)	3318(3)
C16	–853(4)	–1115(6)	3031(3)
C17	–638(3)	516(5)	4201(2)
C18	–809(3)	1572(6)	4574(3)
C21	2404(6)	3565(11)	720(5)
C22	3058(7)	3820(13)	749(6)
C23	3368(4)	4219(10)	1343(5)
C24	2821(5)	4340(9)	1614(4)
C25	190(3)	4742(7)	1190(3)
C26	–56(4)	5939(8)	944(5)
C27	458(5)	6481(7)	691(4)
C28	1036(4)	5737(9)	888(4)

octaethylporphyrinogen, and this prompted us to examine the reaction of **3** with an excess of $CuCl_2$.

The reaction with $CuCl_2$ was carried out on **3**[17] in the presence of an excess of iron required for its preparation. This excess of

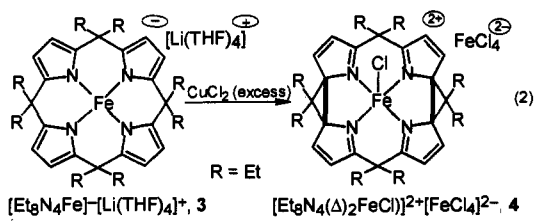

(2)

[Et8N4Fe]–[Li(THF)4]+, 3 [Et8N4(Δ)2FeCl)]2+[FeCl4]2–, 4

iron is responsible for an exchange of counteranions, which in the present case are $[FeCl_4]^{2-}$ rather than $[Cu_4Cl_5]^-$. This leads to the easy conclusion that the bis(cyclopropane) oxidized form of *meso*-octaethylporphyrinogen exists independently of any stabilizing effect assured by the $[Cu_4Cl_5]^-$ cluster. The structure was conclusively established with an X-ray analysis. The simultaneous presence of an iron(II) and an iron(III) atom in the compound makes the magnetic analysis a little bit intriguing. The μ_{eff} has a constant value of 7.2 μ_B from 300 to 30 K, consistent with two noninteracting monomeric species showing a small zero field splitting. In fact, the observed μ_{eff}, though somewhat low, corresponds to a combination of values for iron(II) and iron(III), such a combination ranging normally from 7.5 to 7.9 μ_B. We should mention that $\mu_{eff}{}^2$ and not μ_{eff} is additive.[16]

The oxidation of **1** to **2** and **3** to **4** with the concomitant introduction of two cyclopropane units into the ligand requires some molecular reorganization of the porphyrinogen skeleton, which will be examined by comparison of the structures of **1** and **4**. Copper(II) chloride promotes the four-electron oxidation of the porphyrinogen and leads to the neutral oxidized form containing two cyclopropane units within the porphyrinogen skeleton. The *meso*-octaethylporphyrinogen tetraanion and its oxidized form can be considered as being able to exchange two or four electrons independently of any change in the oxidation state of the metal, as depicted in Scheme 1, though the assistance of the metal plays a crucial role in this chemistry.

The redox chemistry of Co(II)–*meso*-octaalkylporphyrinogen **5** was very helpful in defining the steps (we might synthetically identify) in the conversion of porphyrinogen anion I into the two oxidized forms II and III (Scheme 1). Although all the steps in Scheme 2, except one, have been identified and the corresponding compounds characterized, the sequence shown is not necessarily the best synthetic pathway to reach each compound. Details concerning each step are reported in the Experimental Section. The oxidation of **5** with 1 equiv of $CuCl_2$ led to the corresponding cobalt(III) derivative, **6**. During this reaction, we observed changes in color dependent upon the nature of the solvent, which is related to the disproportionation reaction of **6** (*vide infra* and the Experimental Section). Its magnetic moment μ_{eff} has a value of 3.60 μ_B at 298 K and remains almost constant down to 80 K, then suddenly decreases to 1.10 μ_B at 6 K.[16] Such behavior has much in common with that observed for isoelectronic iron(II) complexes in a square planar coordination.[18] In the latter case these results have been explained by the assumption of an intermediate spin state, $S = 1$, corresponding to a $(d_{xz}d_{yz})^4(d_{xy})^1(d_{z^2})^1$ electronic configuration with a large orbital contribution and a large zero field splitting.

(17) We used the *in situ* preparation of **3** carried out as previously reported for $[Et_8N_4Fe]$-$[Li(MeCN)_4]^+$ in ref 3, with 2 mol of $FeCl_2$ and 1 mol of $[Et_8N_4Li_4(THF)_4]$.

(18) Barraclough, C. G.; Martin, R. L.; Mitra, S.; Sherwood, R. C. *J. Chem. Phys.* **1970**, *53*, 1643.

Table 3. Fractional Atomic Coordinates (×10⁴) for Complex **4**[a]

atom	x/a	y/b	z/c	atom	x/a	y/b	z/c
Fe1	814.1(5)	1601.4(4)	2517.1(10)	C17	408(5)	1798(3)	-588(7)
Fe2	3223.3(8)	3853.6(6)	2191.5(11)	C18	973(5)	1759(3)	-664(7)
Cl1	881(1)	2104(1)	3735(2)	C19	1222(4)	1797(3)	338(7)
Cl2	3411(2)	4359(1)	1074(2)	C20	1846(4)	1762(3)	632(7)
Cl3A	3190(2)	4154(1)	3662(3)	C21	1833(5)	1188(3)	4257(7)
Cl4A	2376(2)	3555(2)	1901(3)	C22	2400(6)	1440(4)	4203(9)
Cl5A	3846(3)	3335(2)	2131(5)	C23	2210(5)	402(4)	3876(8)
Cl3B	2760(26)	4155(20)	2984(47)	C24	2042(6)	214(4)	4879(10)
Cl4B	2944(21)	3346(15)	1601(33)	C25	-747(5)	461(4)	3092(9)
Cl5B	4123(18)	3624(14)	2327(32)	C26A	-1365(9)	599(6)	3235(14)
N1	1624(3)	1295(2)	2091(5)	C26B	-781(15)	260(12)	4134(27)
N2	763(4)	937(2)	3099(5)	C27	-362(4)	1179(4)	4026(8)
N3	-58(3)	1489(3)	2020(6)	C28A	-260(7)	901(6)	5008(13)
N4	821(4)	1858(2)	1015(5)	C28B	-953(13)	1399(10)	4121(22)
C1	1892(4)	1345(3)	1236(7)	C29	-620(5)	2349(4)	94(9)
C2	2207(4)	947(4)	978(7)	C30	-1198(6)	2430(6)	503(12)
C3	2117(4)	638(4)	1702(8)	C31	-74(5)	2459(4)	1764(8)
C4	1761(4)	858(3)	2457(7)	C32	271(7)	2861(5)	1443(9)
C5	1818(4)	792(4)	3585(7)	C33	2238(4)	1739(3)	-297(7)
C6	1262(5)	656(4)	3062(7)	C34	2292(5)	2166(4)	-899(8)
C7	1049(6)	197(4)	2967(8)	C35	2009(4)	2158(3)	1328(8)
C8	476(5)	210(4)	3002(8)	C36	2629(5)	2151(4)	1671(8)
C9	316(5)	674(4)	3074(7)	C41	638(16)	4516(10)	4520(38)
C10	-304(5)	865(4)	3100(8)	C42	238(10)	4303(6)	3671(24)
C11	-376(4)	1131(4)	2163(8)	C43	252(16)	4162(11)	2675(27)
C12	-760(5)	1054(4)	1317(9)	C44	837(22)	4147(14)	2102(35)
C13	-661(5)	1372(4)	651(9)	C45	1280(12)	4367(8)	2924(29)
C14	-226(4)	1675(4)	1062(7)	C46	1203(16)	4541(7)	4024(25)
C15	-197(5)	2171(4)	879(8)	C47	586(19)	4563(14)	5416(28)
C16	288(5)	1891(4)	484(7)	C48	701(21)	4237(11)	2704(30)

[a] The site occupation factors for the disordered atoms are 0.9 for Cl3A, Cl4A, and Cl5A; 0.1 for Cl3B, Cl4B, and Cl5B; 0.6 and 0.4 for the methyl carbons C26 and C28 (A and B, respectively); and 0.5 for the C43, C44, C47, and C48 atoms of the disordered solvent molecules.

Scheme 2

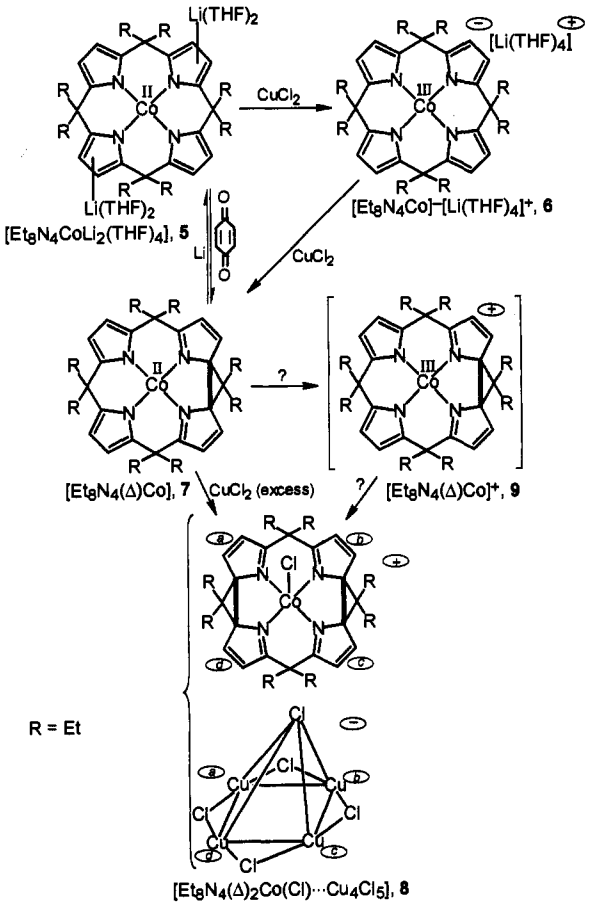

The best access to **7** is not, however, *via* the oxidation with $CuCl_2$ of **6** or *via* our previous synthesis[8] using O_2, a rather low-yield (20%) reaction with the concurrent formation of some secondary compounds. The oxidation of **5** with an excess of *p*-benzoquinone in Et_2O occurs in high yield and allows for the large-scale synthesis of **7**. A synthesis of similar yield can be achieved using I_2 as the oxidizing agent, but the final compound **7** cocrystallized with some LiI. The opening of the cyclopropane unit in **7** can be achieved either by using lithium metal or by the reductive demetalation with H_2S producing *meso*-octaethylporphyrinogen ($Et_8N_4H_4$).

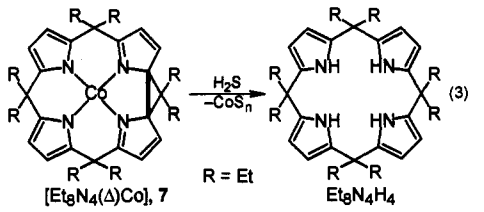

In the further oxidation of **7** by $CuCl_2$ we did not identify the plausible monoelectronic oxidized species **9**, the reaction proceeding directly to **8** independently of the $CuCl_2$:complex stoichiometric ratio. The reaction is an overall two-electron oxidation leading to the introduction of a second cyclopropane unit in the porphyrinogen skeleton. Both cyclopropane units can be reduced in the reductive demetalation carried out on **8** with H_2S. The proposed structure of **8** is based on the X-ray analysis and will be discussed later (*vide infra*). The magnetic moment of **8** (4.70 μ_B at 300 K), which remains constant down to 100 K, is in the expected range for octahedral high-spin cobalt(II) complexes.[15] The relationship among **5**, **6**, and **7** is similar to that discussed for copper (see Scheme 3).[10] The disproportionation of **6** and the reverse reaction, which are solvent dependent, emphasize the occurrence of intermolecular electron-transfer processes which are controlled by the lithium cation and its solvation, as discussed in the preceeding paper. The lithium cation is bound to the porphyrinogen periphery in such a way so as to bridge across two metal complex units.[5,7] Coordinating solvents stabilize the Co(III) form, probably because of the presence of

Table 4. Fractional Atomic Coordinates (×10⁴) for Complex 7

	molecule A			molecule B		
atom	*x/a*	*y/b*	*z/c*	*x/a*	*y/b*	*z/c*
Co1	2018.0(6)	0(–)	–95.3(6)	3086.3(6)	–2380.8(12)	–5045.0(6)
N1	3043(5)	409(7)	–532(5)	1945(4)	–2613(6)	–5283(4)
N2	1363(4)	504(7)	–948(4)	3481(4)	–3016(7)	–5966(4)
N3	1052(5)	–636(6)	349(5)	4192(4)	–1866(6)	–4792(4)
N4	2602(5)	–678(7)	755(4)	2792(4)	–1604(6)	–4129(4)
C1	3829(6)	–74(9)	–408(5)	1295(5)	–1959(9)	–5050(6)
C2	4389(6)	394(11)	–928(7)	570(5)	–2238(10)	–5509(6)
C3	3949(6)	1183(10)	–1378(6)	796(6)	–3110(10)	–6008(6)
C4	3144(5)	1172(8)	–1132(5)	1638(6)	–3304(9)	–5847(7)
C5	2408(6)	1954(9)	–1329(6)	2229(6)	–4249(8)	–6115(6)
C6	1620(5)	1286(8)	–1460(5)	3039(6)	–3808(8)	–6416(5)
C7	992(6)	1315(9)	–2066(5)	3506(7)	–4046(9)	–7063(6)
C8	392(6)	553(10)	–1913(6)	4224(6)	–3422(9)	–7028(5)
C9	596(5)	59(9)	–1213(5)	4221(5)	–2805(9)	–6350(5)
C10	156(6)	–896(9)	–840(6)	4795(6)	–1902(9)	–6119(6)
C11	421(5)	–1100(8)	19(6)	4754(6)	–1563(8)	–5294(6)
C12	72(6)	–1917(8)	535(7)	5329(5)	–734(9)	–4890(7)
C13	503(8)	–1938(9)	1205(7)	5059(6)	–644(9)	–4154(8)
C14	1165(7)	–1083(8)	1139(5)	4342(6)	–1381(9)	–4020(6)
C15	1489(7)	–333(8)	1804(6)	4152(6)	–2076(8)	–3329(6)
C16	2092(6)	–1092(9)	1388(5)	3488(6)	–1267(8)	–3609(6)
C17	2624(8)	–1958(10)	1768(6)	3134(8)	–390(10)	–3122(7)
C18	3341(8)	–1978(10)	1379(6)	2315(7)	–311(10)	–3315(6)
C19	3322(6)	–1153(9)	750(5)	2145(6)	–1059(9)	–3971(6)
C20	4011(6)	–986(9)	175(7)	1311(6)	–1136(10)	–4399(7)
C21	2265(6)	2678(9)	–592(6)	2418(6)	–5003(10)	–5388(6)
C22	3052(8)	3314(12)	–323(10)	1629(8)	–5442(13)	–4952(9)
C23	2630(6)	2633(11)	–2028(6)	1707(6)	–4923(12)	–6761(6)
C24	2037(8)	3597(12)	–2218(9)	2062(9)	–6047(12)	–6946(8)
C25	298(9)	–1932(11)	–1291(7)	4631(10)	–915(13)	–6632(8)
C26	1177(9)	–2294(12)	–1341(8)	3785(13)	–386(12)	–6538(10)
C27	–838(6)	–658(11)	–843(8)	5756(7)	–2226(12)	–6281(8)
C28	–1111(7)	298(12)	–336(9)	6112(8)	–3074(13)	–5728(11)
C29	1245(7)	–708(12)	2608(7)	4652(7)	–1710(12)	–2591(6)
C30	353(10)	–319(15)	2807(8)	5541(8)	–2218(12)	–2536(8)
C31	1574(7)	925(9)	1628(6)	3976(8)	–3302(10)	–3399(7)
C32	2319(10)	1408(12)	2052(10)	3375(11)	–3736(13)	–2887(9)
C33	4844(7)	–640(13)	630(8)	603(8)	–1505(16)	–3779(9)
C34	4741(9)	374(18)	1136(7)	728(10)	–2602(18)	–3483(9)
C35	4148(10)	–2081(12)	–241(8)	1041(9)	9(12)	–4702(9)
C36	3433(10)	–2515(15)	–648(9)	1716(13)	488(14)	–5223(11)

the $[Li(THF)_4]^+$ cation, while the other two forms are preferred in the presence of hydrocarbons.

The introduction of cyclopropane moieties into the porphyrinogen skeleton occurs with significant changes in both the structural and spectroscopic properties of complexes **5**, **7**, and **8**. The bands of 464 and 501 nm in the UV–vis spectrum (Figure 6) are indicative of the presence of a mono(cyclopropane) and a bis(cyclopropane), respectively. The cyclopropane formation parallels the aromatization of *meso*-tetraalkylporphyrinogen to porphyrins, with a significant bathochromic effect.[19] The major differences in the IR spectrum, when the cyclopropane unit is present, are observable in the 3100-, 1600-, and 750-cm^{-1} regions (Figure 7). The structural changes caused by the presence of cyclopropane units in the porphyrinogen skeleton are highlighted by a comparison of the structural parameters of **1**, **4**, **7**, and **8**.

Selected bond distances and angles for complexes **1** and **7** are presented in Tables 6 and 7, respectively. Table 8 compares selected bond parameters for complexes **4** and **8**. In Table 9 the most relevant conformational parameters for complexes **1**, **4**, **7**, and **8** are quoted; the pyrrole rings containing N1, N2, N3, and N4 are labeled A, B, C, and D, respectively. The most relevant parameters concerning the geometry of the atoms related to the formation of cyclopropane are listed for compounds **1**, **4**, **7**, and **8** in Table 10.

An ORTEP drawing and a perspective view of complex **1** are given in Figure 1, top and bottom, respectively. The complex possesses a crystallographically imposed C_2 symmetry with a 2-fold axis running through the iron center and perpendicular to the N_4 core. Two symmetry-related $[Li(THF)_2]^+$ cations are anchored to opposite A and C pyrrole rings. The range of the Li–C and Li–N distances [Li1–C1, 2.457(12) Å; Li1–C2, 2.238(12) Å; Li–C3, 2.387(12) Å; Li–C4, 2.706(13) Å] suggests a Li^+–pyrrole η^3-interaction rather than the alternative η^5-interaction. The geometry of the complex is very close to those observed in the corresponding isostructural derivatives of Cu, Co,[6] and Ni.[10] The N_4 core shows small but significant tetrahedral distortions, with Fe significantly out of the mean plane by 0.063(1) Å (Table 9). The iron atom lies out of the A pyrrole ring by 0.358(1) Å, a distortion which is also observed in the previously cited compounds and is probably related to the anchorage of Li^+. Bond distances and angles within the macrocyclic ligand are in agreement with a π delocalization within the four pyrrole rings.

Complex **4** consists (Figure 2 (top and bottom)) of discrete $[Fe^{III}(\Delta)_2Et_8N_4)Cl]^{2+}$ cations, $FeCl_4^{2-}$ anions (supplementary Figure 1S), and THF and toluene molecules as crystallization solvents. The formation of the two cyclopropane units causes relevant differences in the structural parameters when compared with those of complex **1**. In particular the following can be observed: (i) a remarkable lengthening of the Fe–N bond distances (Table 8); (ii) a strong deviation of the metal from the planar N_4 core; (iii) remarkably larger displacements of the metal from the pyrrole rings; and (iv) a greater bending of the pyrrole rings around the N_4 core. The bending of the pyrrole rings is almost the same, as seen from the values of the dihedral angles (Table 9). This gives rise to a cavity having a cone section conformation,

(19) See ref 11b, Chapters 1 and 5.

Table 5. Fractional Atomic Coordinates (×10⁴) for Complex **8**[a]

atom	x/a	y/b	z/c	atom	x/a	y/b	z/c
Co1	8197(1)	7230(1)	4083(2)	C17	6736(9)	8323(11)	1543(15)
Cl1	9696(2)	7192(3)	4506(4)	C18	6754(9)	7450(12)	843(13)
Cu1A	5533(1)	5760(2)	2382(2)	C19	7443(8)	6997(10)	1519(13)
Cu2A	5585(2)	7628(2)	1667(2)	C20	7668(9)	6006(10)	1148(13)
Cu3A	5521(2)	8821(2)	4310(2)	C21	8789(8)	5260(10)	5114(14)
Cu4A	5438(2)	6968(2)	5049(3)	C22	9104(10)	5443(13)	6404(15)
Cu1B	4770(11)	6149(14)	2313(21)	C23	7404(10)	4416(11)	5065(14)
Cu2B	4858(10)	7554(12)	1843(13)	C24	7727(12)	3499(11)	4338(17)
Cu3B	4809(20)	8359(19)	3961(24)	C25	7010(11)	9028(11)	7671(14)
Cu4B	4688(6)	7015(7)	4381(9)	C26	7270(14)	8840(13)	8817(17)
Cl2	6155(2)	7271(2)	3524(3)	C27	8557(10)	8526(10)	7093(14)
Cl3	4836(3)	6272(3)	823(4)	C28	8910(13)	9470(15)	7440(20)
Cl4	4735(2)	8883(3)	2516(4)	C29	7684(13)	10085(12)	2760(17)
Cl5	4671(3)	8358(3)	5455(4)	C30	7944(15)	10968(14)	3656(23)
Cl6	4587(2)	5744(3)	3698(4)	C31	8958(11)	9137(12)	3439(17)
N1	7734(6)	5943(7)	3195(9)	C32	9323(15)	8926(19)	2296(29)
N2	7681(6)	6933(7)	5427(9)	C33	7253(11)	5498(11)	−105(13)
N3	7725(7)	8563(7)	4745(10)	C34	7553(12)	5733(13)	−1079(14)
N4	7809(6)	7555(7)	2489(9)	C35	8751(9)	5943(10)	1276(13)
C1	7404(8)	5671(10)	2088(13)	C36	9072(11)	4964(12)	1031(17)
C2	6667(8)	5005(8)	1860(14)	O1	5315(8)	7914(10)	8710(12)
C3	6606(9)	4944(9)	2944(14)	C41	4897(15)	8765(17)	8979(22)
C4	7308(8)	5491(9)	3790(13)	C42	3980(17)	8645(21)	9069(27)
C5	7771(9)	5209(9)	4815(12)	C43	3851(16)	7664(21)	8711(27)
C6	7256(7)	6080(9)	5131(12)	C44	4661(15)	7247(15)	8250(20)
C7	6486(8)	6238(10)	5807(13)	C45	1915(21)	6709(19)	1532(33)
C8	6528(8)	7104(10)	6492(12)	C46	1411(23)	6987(26)	2396(34)
C9	7248(8)	7530(10)	6210(11)	C47	1671(22)	7907(30)	3053(32)
C10	7533(9)	8491(11)	6675(13)	C48	2513(21)	7940(27)	2861(37)
C11	7329(9)	8841(9)	5656(12)	C49	2661(20)	7186(33)	1972(41)
C12	6630(8)	9539(10)	5462(14)	C50	962(31)	7327(31)	8302(48)
C13	6647(10)	9602(9)	4382(15)	C51	278(37)	7473(32)	9113(51)
C14	7387(9)	9039(9)	3916(14)	C52	340(34)	8464(40)	9775(33)
C15	7943(11)	9264(11)	3156(15)	C53	1127(45)	8724(32)	9449(47)
C16	7413(9)	8426(10)	2551(14)	C54	1270(31)	8165(47)	8366(53)

[a] The site occupation factors for the disordered Cu atoms are 0.87 for Cu1A and Cu3A; 0.86 for Cu2A; 0.73 for Cu4A; 0.13 for Cu1B and Cu3B; 0.14 for Cu2B; and 0.27 for Cu4B.

Scheme 3

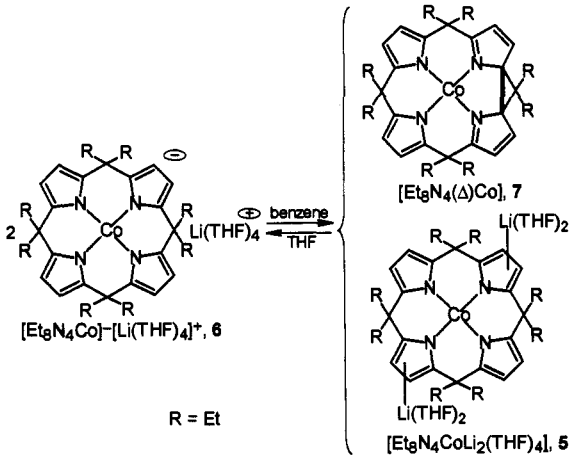

similar to that seen in calix[4]arenes.[9] All of the pyrroles have lost some character of aromaticity, each one showing a system of two localized conjugated double bonds, as indicated by the values of the N1–C1, N2–C9, N3–C11, N4–C19, C2–C3, C7–C8, C12–C13, and C17–C18 bonds and with single bond character for all the other bond distances (Table 8). The configurations at the C4, C6, C14, and C16 asymmetric carbon atoms are *S*, *R*, *S*, and *R*, respectively, with reference to the coordinates of Table 4. Since the space group is centrosymmetric, the enantiomeric diastereoisomer is present in the structure.

The structure of complex **7** (*R*,*S*) consists of [Et$_8$N$_4$(Δ)Co] molecules (Figure 3 (top and bottom)). In the asymmetric unit there are two crystallographically independent molecules (A and B) having similar geometries (the values in square brackets refer to molecule B). The Co–N bond distances fall in a rather narrow range [1.864(8)–1.893(7) Å], and the differences among them are at the limit of significance. The N$_4$ core is planar within experimental error, the cobalt atom deviating by 0.104(1) Å [0.109(1) Å] from the plane (Table 8). Bond distances and angles within the ligand are consistent with a double bond localization on the N3–C11, N4–C19, C12–C13, and C17–C18 bonds of the C and D pyrrole rings involved in the formation of the cyclopropane unit. Accordingly the N3–C14 and N4–C16 distances and the C–C distances adjacent to the macro-ring (C1–C12, C13–C14, C16–C17, and C18–C19) have single bond character (Table 7). This indicates a loss of aromaticity in the C and D rings due to

Table 6. Selected Bond Distances (Å) and Angles (deg) for Complex **1**[a]

Fe1–N1	1.933(5)	C2–C3	1.423(6)
Fe1–N2	1.926(4)	C3–C4	1.383(7)
N1–C1	1.378(7)	C4–C5	1.511(7)
N1–C4	1.387(5)	C5–C6	1.528(7)
N2–C6	1.378(6)	C6–C7	1.377(6)
N2–C9	1.381(7)	C7–C8	1.417(8)
C1–C2	1.392(6)	C8–C9	1.367(6)
C1–C10′	1.515(6)	C9–C10	1.524(6)
N2–Fe1–N2′	175.0(2)	C2–C1–C10′	128.9(4)
N1–Fe1–N2′	90.3(2)	N1–C4–C3	108.5(4)
N1–Fe1–N1′	177.5(2)	C3–C4–C5	131.0(4)
N1–Fe1–N2	89.5(2)	N1–C4–C5	120.4(4)
Fe1–N1–C4	126.0(3)	C4–C5–C6	108.7(4)
Fe1–N1–C1	124.2(3)	N2–C6–C5	119.7(4)
C1–N1–C4	108.3(4)	C5–C6–C7	130.8(4)
Fe1–N2–C9	125.3(3)	N2–C6–C7	109.5(4)
Fe1–N2–C6	127.3(3)	N2–C9–C8	109.2(4)
C6–N2–C9	107.2(4)	C8–C9–C10	129.8(4)
N1–C1–C10′	121.6(4)	N2–C9–C10	120.2(4)
N1–C1–C2	108.8(4)	C1′–C10–C9	112.1(4)

[a] ′ = −*x*, *y*, 0.5 − *z*.

Table 7. Selected Bond Distances (Å) and Angles (deg) for Complex 7

	molecule A	molecule B		molecule A	molecule B
Co1–N1	1.864(8)	1.862(6)	C5–C6	1.503(13)	1.490(14)
Co1–N2	1.871(7)	1.869(7)	C6–C7	1.418(12)	1.369(14)
Co1–N3	1.885(8)	1.899(7)	C7–C8	1.359(15)	1.368(15)
Co1–N4	1.893(7)	1.892(7)	C8–C9	1.369(14)	1.379(13)
N1–C1	1.388(13)	1.367(12)	C9–C10	1.507(15)	1.478(14)
N1–C4	1.395(13)	1.361(13)	C10–C11	1.534(14)	1.467(15)
N2–C6	1.362(12)	1.412(12)	C11–C12	1.447(14)	1.517(14)
N2–C9	1.395(11)	1.376(11)	C12–C13	1.317(16)	1.336(18)
N3–C11	1.269(12)	1.299(12)	C13–C14	1.485(16)	1.470(14)
N3–C14	1.460(12)	1.457(12)	C14–C15	1.537(14)	1.487(15)
N4–C16	1.450(12)	1.458(12)	C14–C16	1.517(14)	1.539(14)
N4–C19	1.278(13)	1.254(12)	C15–C16	1.516(14)	1.513(14)
C1–C2	1.388(15)	1.416(13)	C16–C17	1.492(16)	1.473(16)
C1–C20	1.517(15)	1.497(16)	C17–C18	1.324(17)	1.332(17)
C2–C3	1.408(16)	1.414(16)	C18–C19	1.472(15)	1.465(15)
C3–C4	1.347(13)	1.374(14)	C19–C20	1.493(14)	1.496(14)
C4–C5	1.538(13)	1.560(14)			
N3–Co1–N4	84.2(3)	83.5(3)	Co1–N4–C19	127.9(6)	131.2(6)
N2–Co1–N4	172.7(3)	172.9(3)	Co1–N4–C16	116.9(6)	116.6(5)
N2–Co1–N3	90.4(3)	90.4(3)	C16–N4–C19	110.7(8)	109.1(8)
N1–Co1–N4	90.5(3)	90.2(3)	N1–C1–C20	124.8(8)	127.4(8)
N1–Co1–N3	171.0(3)	169.3(3)	N1–C1–C2	107.9(9)	107.6(8)
N1–Co1–N2	94.2(3)	95.3(3)	C2–C1–C20	127.3(9)	124.9(8)
Co1–N1–C4	125.8(6)	125.3(6)	N1–C4–C3	110.9(8)	111.3(9)
Co1–N1–C1	127.4(7)	125.3(6)	C3–C4–C5	129.8(9)	130.7(9)
C1–N1–C4	106.3(7)	108.0(7)	N1–C4–C5	118.6(8)	117.4(8)
Co1–N2–C9	125.9(6)	128.5(6)	C4–C5–C6	108.3(8)	110.8(8)
Co1–N2–C6	124.1(5)	124.8(6)	N2–C6–C5	123.0(8)	118.8(8)
C6–N2–C9	109.6(7)	106.7(7)	C5–C6–C7	131.3(8)	132.9(9)
Co1–N3–C14	116.1(6)	118.2(5)	N2–C6–C7	105.7(8)	108.3(8)
Co1–N3–C11	130.0(7)	125.7(6)	N2–C9–C8	107.3(8)	108.2(8)
C11–N3–C14	108.7(8)	112.1(8)	C8–C9–C10	127.4(8)	128.3(8)
N2–C9–C10	124.9(8)	122.5(8)	C15–C14–C16	59.5(6)	60.0(7)
C9–C10–C11	114.1(8)	115.3(8)	C14–C15–C16	59.6(7)	61.7(7)
N3–C11–C10	123.1(8)	126.4(9)	C14–C16–C15	60.9(6)	58.3(6)
C10–C11–C12	126.2(8)	125.8(9)	N4–C16–C15	119.8(8)	121.1(8)
N3–C11–C12	110.2(8)	107.7(8)	N4–C16–C14	109.7(7)	110.9(8)
N3–C14–C13	105.1(8)	102.8(8)	C15–C16–C17	125.9(8)	124.6(9)
C13–C14–C16	130.6(9)	134.5(9)	C14–C16–C17	131.2(9)	131.9(9)
C13–C14–C15	126.1(9)	130.0(9)	N4–C16–C17	104.7(8)	104.9(8)
N3–C14–C16	111.1(7)	108.6(8)	N4–C19–C18	108.2(8)	111.0(9)
N3–C14–C15	119.2(8)	116.7(8)	C18–C19–C20	124.5(9)	123.8(9)
C1–C20–C19	113.5(9)	113.9(9)	N4–C19–C20	127.1(9)	125.2(10)

the formation of the cyclopropane unit. The A and B pyrrole rings maintain their aromaticity as seen from the values of bond distances within them. The cyclopropane unit has the expected geometry (Table 10).

The macro-ring assumes a planar conformation, within experimental error, in the case of molecule A, whereas significant tetrahedral distortions are observed in molecule B.[3,6] The differences observed in the dihedral angles between the N_4 plane and the pyrrole rings (Table 9) are small and could be related to the asymmetry of the molecule induced by cyclopropane. The most significant difference within the structural parameters concerns the Co out-of-plane distances from the pyrrole rings, the largest deviations being observed for the C and D rings (Table 9).

The conformation of the ligand leads to two methylenic groups (C21 and C31) being positioned above and two methyl groups (C26 and C36) below the coordination plane. Only one H hydrogen (H311 from the C31 methylenic group) closely approaches the metal at a distance of 2.34 [2.50] Å, the other Co···H contacts being greater than 2.7 Å. These short distances can be viewed as three-center four-electron interactions,[20] or they may arise simply from rigid or sterically constrained ligands.[21]

(20) Anklin, C. G.; Pregosin, P. S. *Magn. Reson. Chem.* **1985**, *23*, 671. Brammer, L.; Charnock, J. M.; Goggin, P. L.; Goodfellow, R. J.; Orpen, A. G.; Koetzle, T. F. *J. Chem. Soc., Dalton Trans.* **1991**, 1789. Wehman-Ooyevaar, I. C. M.; Grove, D. M.; Kooijman, H.; van der Sluis, P.; Speck, A. L.; van Koten, G. *J. Am. Chem. Soc.* **1992**, *114*, 9916.

(21) Sunquist, W. I.; Bancroft, D. P.; Lippard, S. J. *J. Am. Chem. Soc.* **1990**, *112*, 1590.

Table 8. Selected Bond Distances (Å) and Angles (deg) for Complexes 4 and 8 (M = Fe for 4, M = Co for 8)

	4	8		4	8
		(a) In the Porphyrinogen Unit			
M–Cl1	2.233(3)	2.275(3)	C4–C6	1.537(14)	1.611(19)
M–N1	2.167(7)	2.070(10)	C5–C6	1.521(15)	1.501(18)
M–N2	2.159(6)	2.097(12)	C6–C7	1.479(17)	1.512(19)
M–N3	2.152(7)	2.110(10)	C7–C8	1.328(18)	1.348(18)
M–N4	2.152(7)	2.115(12)	C8–C9	1.455(17)	1.461(21)
N1–C1	1.309(12)	1.295(17)	C9–C10	1.547(17)	1.494(22)
N1–C4	1.445(11)	1.400(21)	C10–C11	1.498(16)	1.470(24)
N2–C6	1.435(14)	1.435(17)	C11–C12	1.457(16)	1.518(20)
N2–C9	1.306(14)	1.339(16)	C12–C13	1.331(17)	1.340(26)
N3–C11	1.324(14)	1.290(19)	C13–C14	1.468(16)	1.470(20)
N3–C14	1.451(13)	1.429(21)	C14–C15	1.522(17)	1.479(27)
N4–C16	1.427(14)	1.434(19)	C14–C16	1.562(15)	1.639(21)
N4–C19	1.309(12)	1.290(15)	C15–C16	1.502(16)	1.501(21)
C1–C2	1.449(15)	1.518(19)	C16–C17	1.486(13)	1.437(21)
C1–C20	1.502(13)	1.503(25)	C17–C18	1.317(16)	1.365(22)
C2–C3	1.361(16)	1.358(25)	C18–C19	1.462(14)	1.498(22)
C3–C4	1.463(14)	1.467(17)	C19–C20	1.500(13)	1.503(21)
C4–C5	1.526(13)	1.490(21)			
N3–M–N4	77.1(3)	80.0(4)	C11–N3–C14	107.2(8)	109.9(12)
N2–M–N4	132.2(3)	142.0(4)	M–N4–C19	126.8(6)	124.3(10)
N2–M–N3	85.0(3)	87.1(4)	M–N4–C16	118.9(6)	117.9(9)
N1–M–N4	84.4(3)	87.5(4)	C16–N4–C19	106.2(8)	107.2(11)
N1–M–N3	131.5(3)	140.4(4)	N1–C1–C20	122.2(8)	125.1(13)
N1–M–N2	75.1(2)	79.9(4)	N1–C1–C2	110.5(8)	111.3(12)
M–N1–C4	119.5(5)	118.8(9)	C2–C1–C20	127.3(8)	123.5(12)
M–N1–C1	126.1(6)	124.6(10)	N1–C4–C3	107.9(8)	108.2(12)
C1–N1–C4	107.3(7)	108.2(11)	C3–C4–C6	127.2(9)	127.0(11)
M–N2–C9	127.0(6)	124.3(10)	C3–C4–C5	124.9(8)	121.3(13)
M–N2–C6	119.7(6)	117.1(8)	N1–C4–C6	112.2(8)	112.6(11)
C6–N2–C9	106.0(8)	107.3(10)	N1–C4–C5	118.2(8)	122.6(11)
M–N3–C14	117.5(6)	117.8(9)	C5–C4–C6	59.6(6)	57.7(9)
M–N3–C11	127.3(7)	124.2(10)	C4–C5–C6	60.6(6)	65.2(9)
C4–C6–C5	59.9(6)	57.1(9)	C13–C14–C15	125.9(9)	124.4(14)
N2–C6–C5	120.3(9)	121.0(10)	N3–C14–C16	113.2(8)	112.5(12)
N2–C6–C4	112.8(9)	111.6(10)	N3–C14–C15	120.8(8)	122.5(13)
C5–C6–C7	125.1(10)	124.4(13)	C15–C14–C16	58.3(7)	57.3(10)
C4–C6–C7	125.4(9)	129.5(11)	C14–C15–C16	62.2(7)	66.7(11)
N2–C6–C7	106.9(9)	106.6(11)	C14–C16–C15	59.5(7)	56.0(10)
N2–C9–C8	112.8(10)	111.3(12)	N4–C16–C15	120.7(8)	120.0(13)
C8–C9–C10	126.7(10)	128.9(12)	N4–C16–C14	112.5(8)	111.6(12)
N2–C9–C10	120.4(10)	119.8(11)	C15–C16–C17	125.8(10)	124.7(15)
C9–C10–C11	106.6(9)	104.7(12)	C14–C16–C17	122.7(9)	128.5(13)
N3–C11–C10	119.9(9)	123.3(13)	N4–C16–C17	107.7(9)	107.9(13)
C10–C11–C12	129.1(10)	127.7(12)	N4–C19–C18	111.4(8)	112.0(13)
N3–C11–C12	111.0(10)	108.9(12)	C18–C19–C20	127.8(9)	124.7(13)
N3–C14–C13	105.7(8)	106.3(13)	N4–C19–C20	120.8(8)	123.3(13)
C13–C14–C16	126.8(9)	127.0(13)	C1–C20–C19	105.6(8)	104.0(12)

(b) In the $Cu_4Cl_5^-$ Unit (Complex 8)

Cu1A–Cl2	2.493(4)	Cu3A–Cl2	2.505(4)
Cu1A–Cl3	2.332(6)	Cu3A–Cl4	2.321(5)
Cu1A–Cl6	2.330(5)	Cu3A–Cl5	2.336(6)
Cu1A–C2	2.112(13)	Cu3A–C12	2.143(13)
Cu1A–C3	2.160(15)	Cu3A–C13	2.152(16)
Cu2A–Cl2	2.475(5)	Cu4A–Cl2	2.467(6)
Cu2A–Cl3	2.329(5)	Cu4A–Cl5	2.350(5)
Cu2A–Cl4	2.338(5)	Cu4A–Cl6	2.390(5)
Cu2A–C17	2.179(17)	Cu4A–C7	2.149(15)
Cu2A–C18	2.157(16)	Cu4A–C8	2.174(13)
C2–Cu1A–C3	37.0(6)	C12–Cu3A–C13	36.4(6)
Cl3–Cu1A–Cl6	112.6(2)	Cl4–Cu3A–Cl5	113.2(2)
Cl2–Cu1A–Cl6	95.2(2)	Cl2–Cu3A–Cl5	93.1(2)
Cl2–Cu1A–Cl3	93.0(2)	Cl2–Cu3A–Cl4	95.5(2)
C17–Cu2A–C18	36.7(6)	C7–Cu4A–C8	36.3(5)
Cl3–Cu2A–Cl4	116.0(2)	Cl5–Cu4A–Cl6	113.8(2)
Cl2–Cu2A–Cl4	95.9(2)	Cl2–Cu4A–Cl6	94.3(2)
Cl2–Cu2A–Cl3	93.5(2)	Cl2–Cu4A–Cl5	93.7(2)

This is consistent with the closest approach of C31 to the metal (Co···C31, 3.235(11) [3.308(12)] Å; Co···C21, 3.409(11) [3.425-(12)] Å; Co···C26, 3.746(11) [3.709(10)] Å; Co···C36, 3.930-(11) [4.133(11)] Å). All of these features are comparable with those observed in the corresponding Ni and Cu derivatives.

The configurations of the two asymmetric carbon atoms are *R* for C14 and *S* for C16 with reference to the coordinates of

Table 9. Comparison of Structural Parameters for Complexes **1**, **4**, **7**, and **8** (M = Fe for **1** and **4**, M = Co for **7** and **8**)

	1	**4**	**7**[a]	**8**
dist of atoms from N_4 core (Å)	N1, 0.021(4)	N1, 0.006(6)	N1, 0.019(9) [0.034(7)]	N1, 0.011(10)
	N2, –0.021(4)	N2, –0.006(6)	N2, –0.017(8) [–0.043(8)]	N2, –0.011(10)
	N1′, 0.021(4)	N3, 0.011(9)	N3, 0.016(8) [0.037(7)]	N3, 0.014(11)
	N2′, –0.021(4)	N4, –0.006(6)	N4, –0.018(8) [–0.037(7)]	N4, –0.011(10)
	M, 0.063(1)	M, –0.878(1)	M, –0.104(1) [–0.109(1)]	M, –0.696(2)
dist of M from N1,C1···C4 ring (A) (Å)	0.358(1)	0.932(1)	0.202(1) [0.381(1)]	1.001(2)
dist of M from N2,C6···C9 ring (B) (Å)	0.127(1)	0.921(1)	0.220(1) [0.077(1)]	1.072(2)
dist of M from N3,C11···C14 ring (C)[b] (Å)	0.358(1)	0.959(1)	0.715 (1) [0.718(1)]	1.036(2)
dist of M from N4,C16···C19 ring (D)[b] (Å)	0.127(1)	1.029(1)	0.679(1) [0.507(1)]	1.076(2)
dihedral angles between the N_4 core and the	(A) 147.2(1)	130.7(3)	156.5(3) [153.8(3)]	131.5(4)
A, B, C, and D pyrrole rings (deg)	(B) 149.5(1)	131.1(3)	154.7(3) [158.4(3)]	130.8(4)
	(C)[b] 147.2(1)	129.3(3)	147.6(3) [147.0(3)]	131.4(4)
	(D)[b] 149.5(1)	127.9(3)	149.4(3) [155.2(3)]	130.6(4)

[a] Values for molecule B are in square brackets. [b] For complex **1**, the C and D rings are the symmetry-related ones.

Table 10. Structural Parameters Related to the Formation of the Cyclopropane Unit in Complexes **1**, **4**, **7** and **8**[a]

	1		**1**
C4···C6 (Å)	2.469(6)	C4–C5–C6 (deg)	108.7(4)
C9···C1′ (Å)	2.520(5)	C9–C10–C1′ (deg)	112.1(4)

		7		
	4	molecule A	molecule B	**8**
C1···C19 (Å)	2.391(13)	2.517(13)	2.509(14)	2.369(25)
C4···C6 (Å)	1.537(14)	2.465(11)	2.512(14)	1.611(19)
C9···C11 (Å)	2.441(16)	2.552(14)	2.488(14)	2.346(23)
C14···C16 (Å)	1.562(15)	1.517(14)	1.539(14)	1.639(21)
C4–C5–C6 (deg)	60.6(6)	108.3(8)	110.8(8)	57.7(9)
C9–C10–C11 (deg)	106.6(9)	114.1(8)	115.3(8)	104.7(12)
C14–C15–C16 (deg)	62.2(7)	59.6(7)	61.7(7)	66.7(11)
C1–C20–C19 (deg)	105.6(8)	113.5(9)	113.9(9)	104.0(12)

[a] ′ = $-x, y, {}^1/_2 - z$.

Table 2. Since the space group is acentric this is the only diastereoisomer present in the structure, the absolute configuration having been unambiguously established by X-ray analysis (see the Experimental Section). It corresponds to that present in the Cu derivative, and it is also the enantiomer of that found in the Ni derivative.[10] For discussion on this solid-state self-resolution refer to the preceding paper and related references.[22]

The structure of complex **8** consists of a discrete $[Et_8N_4(\Delta)_2\text{-}CoCl]^+$ cation (Figure 4 (top and bottom))[15] having a $Cu_4Cl_5^-$ counteranion, each copper(I) being η^2-bonded to the terminal double bonds of the pyrrole ring. The geometry of the cation is very close to that observed in complex **4** (Tables 8 and 9). In particular, the molecule shows a cavity having a cone section conformation with two double bonds localized within each pyrrole ring.

The anion seems to take advantage of this conformation, which does not seem to be determined, however, by the copper(I)–η^2-pyrrole interaction. The most relevant parameters are compared in Tables 8–10 with those of complex **4**, indicating no remarkable differences between them.

In these two compounds a strong displacement of the metal atom from the N_4 core is observed along with a strong deformation of the bond angles around the metal, the N–M–N angles in the five-membered chelating rings being narrower than those in the six-membered chelation rings. The N–M–N angles involving opposite nitrogen atoms deviate dramatically from 180°. On moving from complex **1** to complexes **4** and **8**, the N_4 core undergoes a significant deformation from a square of 2.73 Å (mean value) on one edge to a larger rectangle of 2.68 × 2.91 Å (mean values) in dimension, indicating that the M out-of-plane displacements could not be attributed to a variation in size of the N_4 core but mainly to the presence of chlorine in the fifth coordination site.

(22) (a) Jacques, J.; Collet, A.; Wilen, S. H. *Enantiomers, Racemates and Resolutions*; Wiley: New York, 1981; pp 14–18. (b) Caswell, L.; Garcia-Garibay, M. A.; Scheffer, J. R.; Trotter, J. *J. Chem. Educ.* **1993**, *70*, 785.

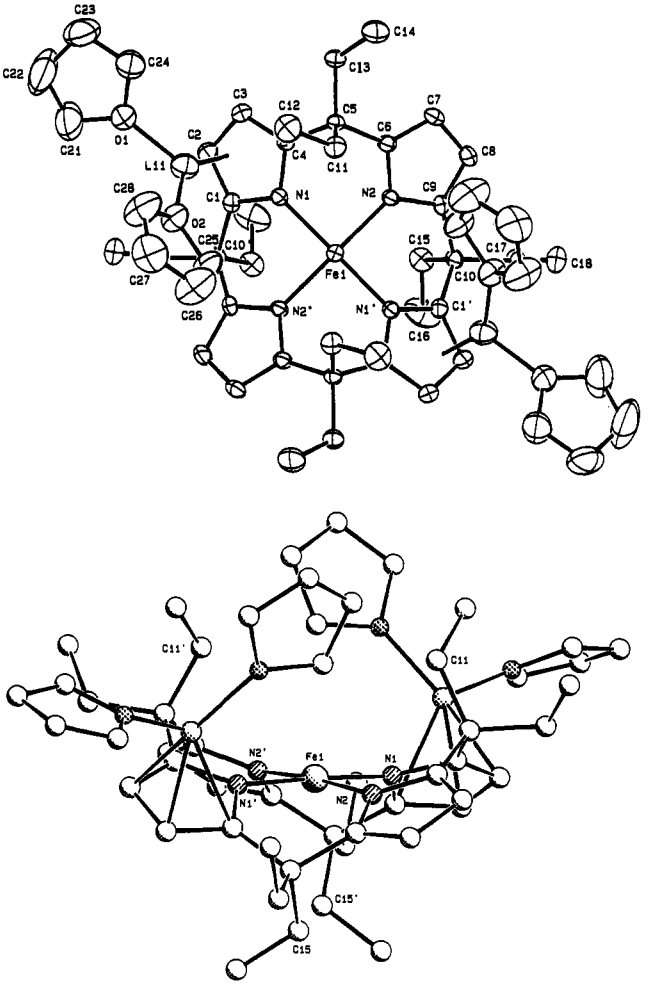

Figure 1. (top) ORTEP view of complex **1** (30% probability ellipsoids). Primes denote a transformation of $-x, y, 0.5 - z$. (bottom) A perspective view (SCHAKAL) of complex **1**.

The configurations at the C4, C6, C14, and C16 asymmetric carbon atoms are the same as those observed for complex **4**.

The $Cu_4Cl_5^-$ anion is disordered, the four copper atoms being statistically distributed over two positions (see the Experimental Section). Figure 5 shows the four possible statistical distributions. Each copper center possesses an approximately trigonal-pyramid coordination environment wherein the "alkene" ligand is considered to occupy one coordination site.[23] The Cl2 chlorine atom capping the Cu_4 square points toward the center of the cavity, but it does not interact with the cobalt atom, the Co···Cl2 separation being 3.097(3) Å. The Cl2···C distances are greater than 3.26 Å.

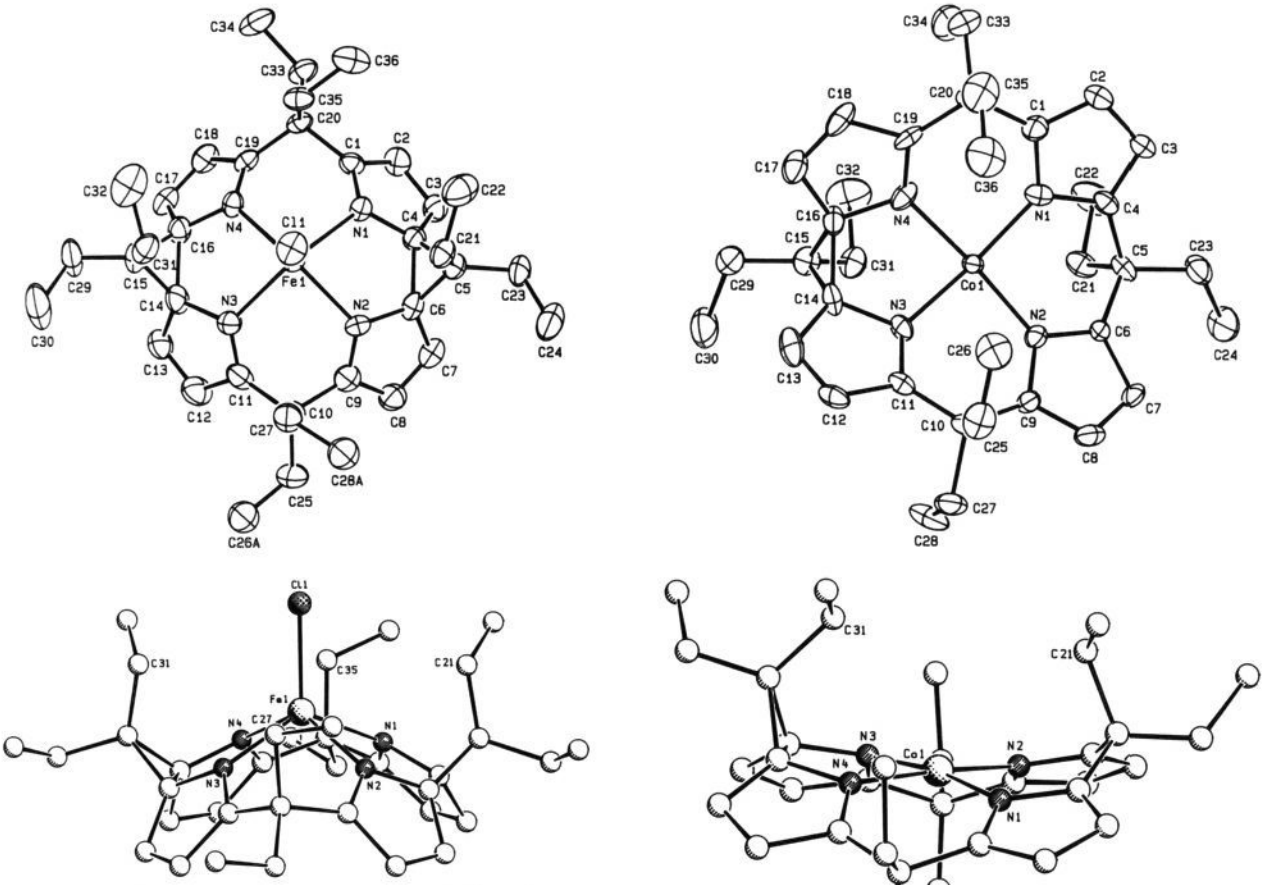

Figure 2. (top) ORTEP view of complex **4** (30% probability ellipsoids). (bottom) A perspective view (SCHAKAL) of complex **4**.

Figure 3. (top) ORTEP view of molecule A in complex **7** (30% probability ellipsoids). (bottom) A perspective view (SCHAKAL) of complex **7** (molecule A).

Conclusions

The discovery of the oxidative transformations of *meso*-octaalkylporphyrinogen into structures containing cyclopropane units may provide interesting information about the preliminary steps of porphyrinogen aromatization to porphyrins. The relatively easy formation and cleavage of the cyclopropane unit within the porphyrinogen skeleton shows how redox processes based exclusively on the ligand, on the metal, or on the metal–ligand sites can occur in metal–porphyrinogen complexes. This is particularly emphasized in the stepwise redox process leading to the formation and rupture of one, then two, cyclopropane moieties, with the isolation and structural characterization of several intermediates. The reactivity of the cyclopropane unit should allow interesting modifications of the porphyrinogen skeleton, including the access to the corrinoid-type frame.

Experimental Section

General Procedure. All reactions were carried out under an atmosphere of purified nitrogen. Solvents were dried and distilled before use by standard methods. The syntheses of $Et_8N_4H_4$,[5] $[Et_8N_4Li_4(THF)_4]$,[5] $[Et_8N_4CoLi_2(THF)_4]$,[6] and $[Et_8N_4FeLi_2(THF)_4]$[6] were carried out as previously reported. The experimental procedure we often used is the extraction of the solid products with the mother liquor following the workup reported in ref 24. Infrared, UV–vis, and ^1H NMR spectra were recorded with a Perkin-Elmer 1600 FT–IR spectrophotometer, HP 8452A diode array spectrophotometer, and 200-AC Bruker instrument, respectively. Magnetic susceptibility measurements were made with a Quantum Design Model MPMS5 SQUID magnetometer at a magnetic field strength of 3 kOe, in the temperature range 6–310 K. Corrections were applied for diamagnetism calculated from Pascal constants. Effective magnetic moments were calculated by the equation $\mu_{eff} = 2.828(\chi_{Fe}T)^{1/2}$, where χ_{Fe} is the magnetic susceptibility *per* iron.

Preparation of 2. $FeCl_2{\cdot}(THF)_{1.5}$ (0.84 g, 3.60 mmol) was added very slowly to a THF (300 mL) solution of $[Et_8N_4Li_4(THF)_4]$ (3.50 g, 4.10 mmol). A yellow-orange solution formed which was stirred for 2 h. The solution was then reacted with solid $CuCl_2{\cdot}(THF)_{0.5}$ (2.80 g, 16.4 mmol). The resulting deep-red solution was evaporated to dryness, and the residue was extracted with toluene (250 mL). The undissolved solid was filtered off. When the toluene was evaporated to 50 mL, **2** precipitated as orange crystals (50%). The solid contains toluene of crystallization. Anal. Calcd for $C_{36}H_{48}Cl_6Cu_4FeN_4{\cdot}(C_7H_8)_{1.5}$: C, 46.61; H, 4.01; N, 4.68. Found: C, 46.20; H, 3.91; N, 4.37. UV–vis (THF): λ 250 nm (ϵ 19 860 cm^{-1} M^{-1}), 298 (20 950), 298 (19 960). IR (Nujol): ν 3068, 1562, 1537 cm^{-1}.

Preparation of 4. $FeCl_2{\cdot}(THF)_{1.5}$ (1.90 g, 8.20 mmol) was added slowly to a THF (300 mL) solution of $[Et_8N_4Li_4(THF)_4]$ (3.50 g, 4.10 mmol). The resulting deep-red solution was stirred for 2 h, then reacted with $CuCl_2{\cdot}(THF)_{0.5}$ (3.60 g, 21.20 mmol). The reaction led to a bright-red solution which was stirred for 1 day at room temperature. The solution was evaporated to dryness, and the residue was extracted with toluene (200 mL). The undissolved solid was filtered off. When toluene was evaporated to 50 mL, **4** was collected as an amber solid (20%). The crystals contained C_7H_8 and THF of crystallization. Anal. Calcd for $C_{36}H_{48}ClFeN_4{\cdot}FeCl_4{\cdot}(C_7H_8)_{0.5}{\cdot}(C_4H_8O)_{0.5}$: C, 55.02; H, 6.24; N, 6.19. Found: C, 55.82; H, 6.21; N, 6.34. μ_{eff} = 7.2 μ_B/mol with a constant value from 298 to 30 K. UV-vis (THF): λ 252 nm (ϵ 10 000 cm^{-1} M^{-1}), 310 (12 700), 383 (8000), 486 (1670). IR (Nujol): ν 3094, 1570, 1567 cm^{-1}.

Preparation of 6 from the Oxidation of 5 with $CuCl_2$. $CuCl_2{\cdot}(THF)_{0.5}$ (0.125 g, 0.72 mmol) was added to a THF (100 mL) solution of **5** (0.64

(23) For olefinic copper(I) complexes, see: Thompson, J. S.; Swiatek, R. W. *J. Am. Chem. Soc.* **1985**, *107*, 110. Munakata, M.; Endicott, J. F. *Inorg. Chem.* **1984**, *23*, 3693.

(24) Floriani, C.; Mange, V. In *Inorganic Syntheses*, Angelici, R. J., Ed.; Wiley: New York, 1990; Vol. 28, pp 263–267.

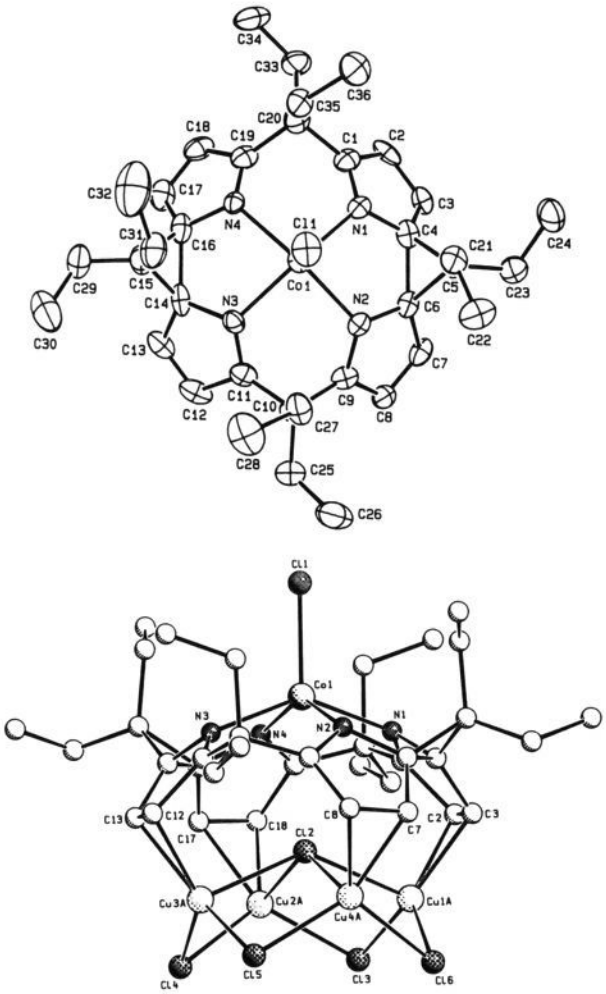

Figure 4. (top) ORTEP view of complex **8** (30% probability ellipsoids). For clarity the $Cu_4Cl_5^-$ moiety is omitted. (bottom) A perspective view (SCHAKAL) of complex **8**.

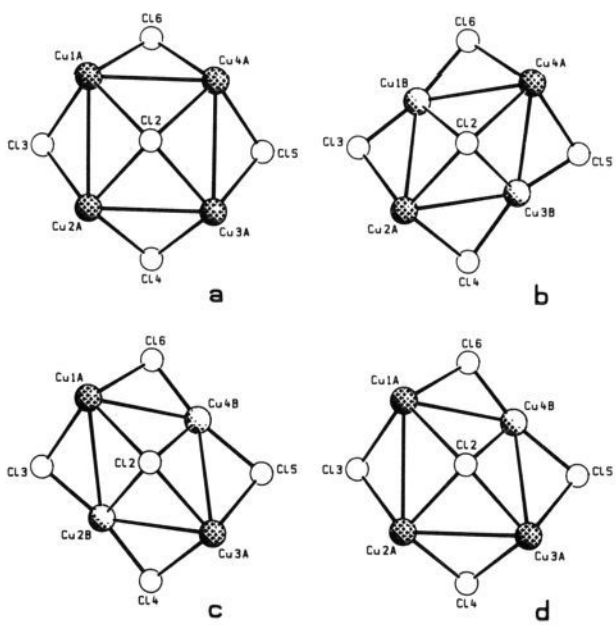

Figure 5. Four possible statistical distributions in the $Cu_4Cl_5^-$ anion: (a) 60%; (b) 13%; (c) 14%; (d) 13%.

g, 0.71 mmol). A violet solution rapidly formed with some insoluble solid. The suspension was left to stand for 1 day, then the solution was evaporated to dryness. The solid residue was treated with toluene (150 mL) and the undissolved solid filtered off. The toluene solution, which had a brown-green color, was evaporated to dryness. The solid residue, dissolved in THF, gave a violet solution which, upon addition of *n*-heptane, gave crystals of **6** (68%). Anal. Calcd for $C_{52}H_{80}CoLiO_4$: C, 70.00; H, 9.05; N, 6.29. Found: C, 69.90; H, 8.68; N, 6.51. μ_{eff} was 3.60 μ_B at 298 K, constant down to 80 K, then decreased to 1.10 μ_B at 6 K.

Preparation of 6 from the Reaction of 5 and 7. THF (70 mL) was added to a solid mixture of **5** (1.14 g, 1.30 mmol) and **7** (0.77 g, 1.30 mmol). A violet solution rapidly formed. The addition of *n*-hexane (30 mL) gave violet crystals of **6** (65%).

Preparation of 7 Using *p*-Benzoquinone. A Et_2O (250 mL) solution of *p*-benzoquinone (4.90 g, 45.0 mmol) was added dropwise to a Et_2O (300 mL) solution of **5** (10.2 g, 11.4 mmol). A mixed brown-green and blue solid formed. The suspension was stirred for 1 day, then the solid was extracted with the mother liquor. The solution was evaporated to dryness, the solid residue was washed with *n*-hexane, and the product was collected (83%). Crystals suitable for X-ray analysis were obtained from a dilute solution in Et_2O. Anal. Calcd for $C_{36}H_{48}CoN_4$: C, 72.60; H, 8.10; N, 9.40. Found: C, 72.82; H, 8.23; N, 9.21. μ_{eff} = 2.70 μ_B at 298 K and 2.40 μ_B at 6 K. UV–vis (THF): λ 246 nm (ϵ 32 170 cm^{-1} M^{-1}), 462 (6822). IR (Nujol): ν 3096, 3079, 1595 cm^{-1}.

Preparation of 7 from the Oxidation of 5 with O_2. A toluene (50 mL) solution of **5** (1.0 g, 1.11 mmol) was saturated with O_2. The solution darkened in a few minutes, then some solid precipitated. The suspension was stirred overnight. The red-brown solid was filtered off, then the volume of the filtrate was reduced to 20 mL. Cooling the solution for 1 week at −10 °C afforded green crystals of **7** (20%).

Preparation of 7 from the Oxidation with Iodine. Iodine (0.20 g, 0.70 mmol) was added to a Et_2O (70 mL) solution of **5** (0.60 g, 0.70 mmol). A dark solution was obtained with some white solid (LiI) which was removed by filtration. The solution, evaporated to 20 mL, gave crystals of **7** cocrystallized with some LiI. The IR spectrum was superimposable with that from the alternative preparation. Anal. Calcd for $C_{36}H_{48}CoN_4(LiI)_{0.4}$: C, 66.60; H, 7.45; N, 8.63. Found: C, 66.36; H, 7.70; N, 8.43.

Reduction of 7 with Lithium Metal. A THF (70 mL) solution of **7** (1.15 g, 1.90 mmol) was reacted with lithium metal (0.061 g, 8.70 mmol) under argon. A red solution was obtained after 1 day of stirring. The excess lithium was removed by filtration, then *n*-heptane (50 mL) was added. Complex **5** precipitated as a microcrystalline solid, which was recrystallized from toluene (70%).

Reductive Demetalation of 7 with H_2S. A THF (50 mL) solution of **7** (1.0 g, 1.7 mmol) was saturated with H_2S. In 4 h the solvent became red-brown and a black solid precipitated. The solvent was evaporated to dryness and the residue extracted with *n*-hexane (50 mL). The suspension was filtered, and the *n*-hexane solution evaporated to dryness gave 85% of $Et_8N_4H_4$.

Preparation of 8. $CuCl_2{\cdot}(THF)_{0.5}$ (2.0 g, 11.7 mmol) was added to a THF (70 mL) green-brown suspension of **7** (1.45 g, 2.4 mmol). The suspension was stirred for 1 day, then the solid was filtered off. The red solution gave, upon addition of *n*-heptane and cooling to −4 °C, red crystals of **8** (35%). Anal. Calcd for $C_{44}H_{64}Cl_6CoCu_4N_4O_2$: C, 43.78; H, 5.30; N, 4.64. Found: C, 43.58; H, 5.25; N, 4.64. UV–vis (THF): λ 256 nm (ϵ 25 185 cm^{-1} M^{-1}), 306 (33 016), 502 (8599). IR (Nujol): ν 3100, 1598, 1544 cm^{-1}.

Reductive Demetalation of 8 with H_2S. A THF (50 mL) solution of **8** (0.17 g, 0.14 mmol) was saturated with H_2S. A green suspension rapidly formed which was stirred for 2 h. The solvent was evaporated to dryness and the residue extracted with *n*-hexane (50 mL). The solid was filtered off, and the *n*-hexane solution evaporated to dryness gave 85% of $Et_8N_4H_4$.

X-ray Crystallography for Complexes 1, 4, 7, and 8. The crystals of compounds **1**, **4**, **7**, and **8** were mounted in glass capillaries, and the capillaries were sealed under nitrogen. The reduced cells were obtained with the use of TRACER.[25] Crystal data and details associated with structure refinement are given in Table 1. Data were collected at room temperature (295 K) on a single-crystal diffractometer. For intensities and background individual reflection profiles were analyzed.[26] The structure amplitudes were obtained after the usual Lorentz and polarization corrections and the absolute scale was established by the Wilson

(25) Lawton, S. L.; Jacobson, R. A. *TRACER (a cell reduction program)*; Ames Laboratory, Iowa State University of Science and Technology: Ames, IA, 1965.

(26) Lehmann, M. S.; Larsen, F. K. *Acta Crystallogr., Sect. A: Cryst. Phys., Diffr., Theor. Gen. Crystallogr.* **1974**, *A30*, 580–584.

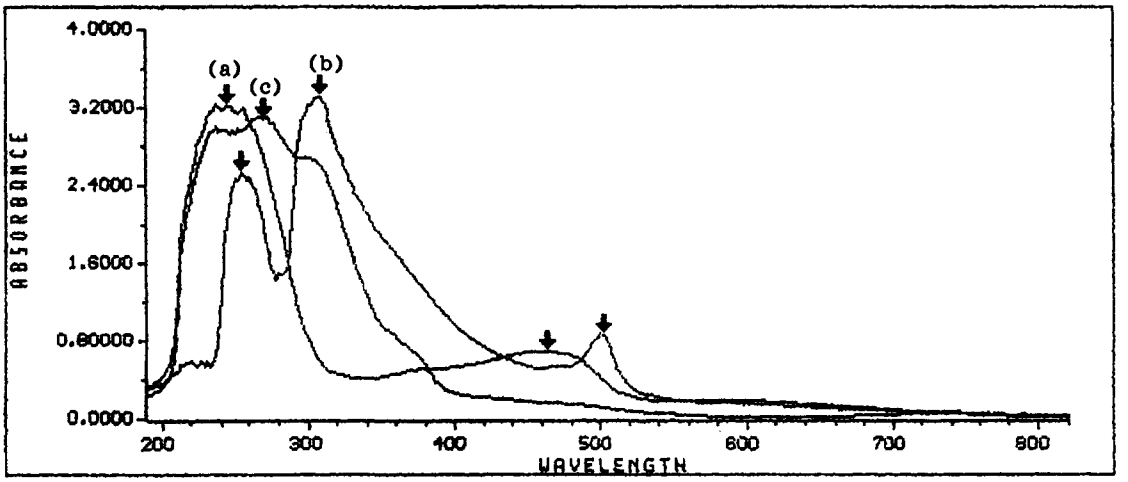

(a) = complex **7**
(b) = complex **8**
(c) = complex **5**

Figure 6. UV–vis spectra of complexes **5**, **7**, and **8** in THF solution (10^{-3} M).

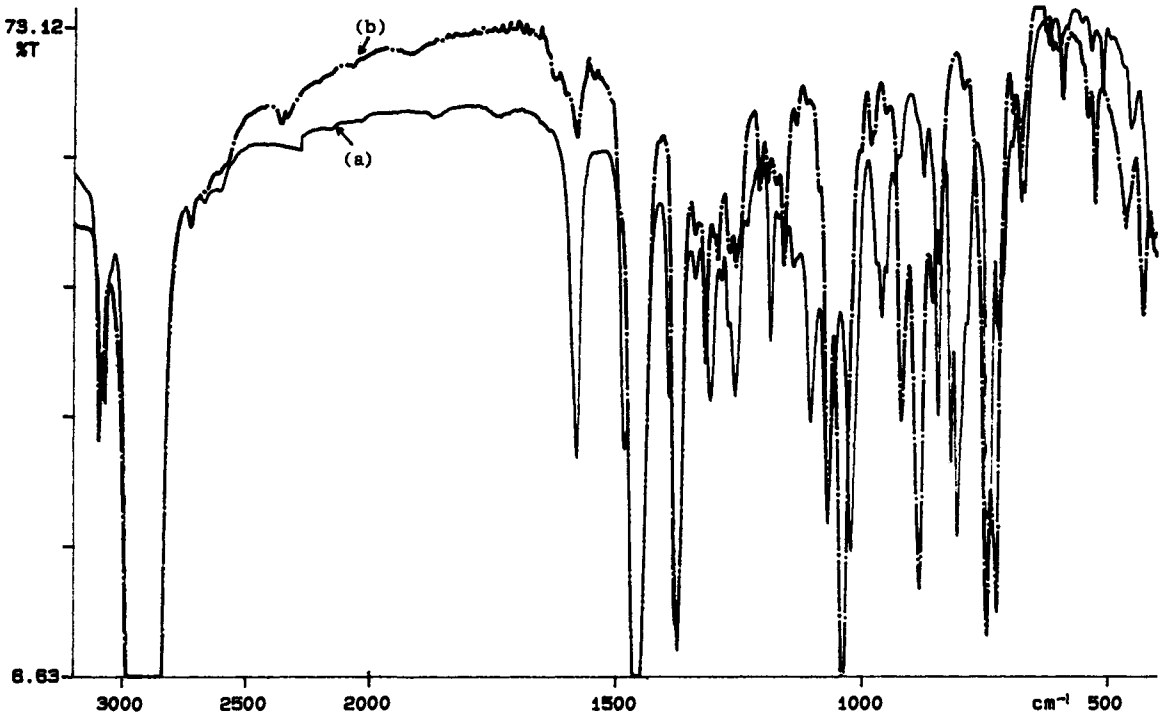

IR (nujol) (a): Complex **6**
(b): Complex **7**

Figure 7. Comparison between the IR spectra of complexes **6** and **7**.

method.[27] Data were corrected for absorption using the program ABSORB[28] for complex **1** and a semiempirical method[29] for complexes **4**, **7**, and **8**. The function minimized during the full-matrix least-squares refinement was $\sum w|\Delta F|^2$. A weighting scheme $w = k/[\sigma^2(F_o) + g|F_o|^2]$ based on counting statistics was applied for complexes **1**, **4**, and **7**.[30] For complex **8** unit weights were applied since these gave the most satisfactory analysis of variance and the best agreement factors. Anomalous scattering corrections were included in all structure factor calculations.[31b] Scattering factors for neutral atoms were taken from ref 31a for non-hydrogen atoms and from ref 32 for H. Among the low-angle reflections no correction for secondary extinction was deemed necessary. All calculations were carried out on an IBM-AT personal computer equipped with an INMOS T800 Transputer and an ENCORE 91 computer using SHELX-76.[30] Solution and refinement were based on the observed reflections. The structures were solved by the heavy-atom method starting from a three-dimensional Patterson map.

Complex 1. Refinement was done first isotropically, then anisotro-

(27) Wilson, A. J. C. *Nature* 1942, *150*, 151.
(28) Ugozzoli, F. ABSORB, a Program for F_o Absorption Correction. *Comput. Chem.* **1987**, *11*, 109.
(29) North, A. C. T.; Phillips, D. C.; Mathews, F. S. *Acta Crystallogr., Sect. A: Cryst. Phys., Diffr., Theor. Gen. Crystallogr.* **1968**, *A24*, 351.
(30) Sheldrick, G. M. *SHELX-76: System of Crystallographic Computer Programs*; University of Cambridge: Cambridge, England, 1976.
(31) (a) *International Tables for X-ray Crystallography*; Kynoch Press: Birmingham, England, 1974; Vol. IV, p 99. (b) Ibid. p 149.
(32) Stewart, R. F.; Davidson, E. R.; Simpson, W. T. *J. Chem. Phys.* **1965**, *42*, 3175.

pically, for all non-H atoms. All the hydrogen atoms were located from difference Fourier maps and introduced in the final refinement as fixed atom contributions (isotropic U's fixed at 0.10 Å^2). The final difference map showed no unusual features, with no significant peaks above the general background.

Complex 4. Refinement was done first isotropically, then anisotropically, for all non-H atoms of the complex molecule and $FeCl_4^{2-}$ anion, down to $R = 0.080$. A difference Fourier map, calculated at this stage, revealed some residual significant peaks in the regions of the ethylic chains bonded to the C10 *meso*-carbon and the $FeCl_4^{2-}$ anion. These peaks, along with the high values reached by the U_{ij} thermal parameters of the C26 and C28 methyl carbons and the chlorine atoms, suggested a disordered distribution of these groups. The disorder was solved in terms of "partial" atoms by considering the C26 and C28 methyl carbons and the Cl3, Cl4, and Cl5 chlorine atoms distributed over two positions (A and B). The A positions of the chlorine atoms (site occupation factor of 0.9) were then anisotropically refined, while the B position (site occupation factor of 0.1) as well as the C26 and C28 positions (A and B) were isotropically refined. The Fe···Cl distances involving chlorines in B positions fall in a rather wide range (1.76(6)–2.20(4) Å), indicating a disorder, which could not be solved, involving the iron atom (Fe2) too. This model could be satisfactorily refined with no residual peaks in the final difference Fourier maps. Further troubles were encountered in the definition of the crystallization solvent molecule. In the initial stage it was considered as a toluene molecule, but the refinement did not converge. The ΔF map showed a significant residual peak (C48) occupying a fifth position of a THF molecule sharing the C42, C41, C46, and C45 atoms with toluene. This model, implying a disordered distribution between toluene (50%) and THF (50%), was successfully refined to convergence anisotropically for the shared atoms and isotropically for C43, C44, C47, and C48. The site occupation factors of the disordered atoms are given in Table 3. All the hydrogen atoms, but those associated to the solvent molecules, which were ignored, were located from difference Fourier maps and introduced in the final refinement as fixed atom contributions (isotropic U's fixed at 0.12 Å^2). The final difference map showed no unusual features, with no peaks above the general background.

Complex 7. Refinement was done first isotropically, then anisotropically, for all non-H atoms. All the hydrogen atoms, partly located from ΔF maps, partly put in geometrically calculated positions, were introduced in the final refinement as fixed atom contributions (isotropic U's fixed at 0.08 Å^2). Since the space group is acentric, the crystal chirality was tested by inverting all the coordinates ($x, y, z \rightarrow -x, -y, -z$) and refining to convergence once again. The resulting R values [R = 0.071 and R_G = 0.100 for the inverted structure *vs* R = 0.069 and R_G = 0.098 for the original choice] indicated the previous choice should be considered the correct one. The coordinates quoted in Table 4 refer to the original choice. The final difference map showed eight peaks (of about 1.0 Å^{-3}) at ≈1 Å from cobalt atoms in the directions of the nitrogen atoms.

Complex 8. Refinement was done first isotropically, then anisotropically, for all the non-H atoms. All the hydrogen atoms of the complex molecule were located from difference Fourier maps and introduced in the final refinement as fixed atom contributions (isotropic U's fixed at 0.12 Å^2). The H atoms attached to the C41–C44 carbons of a THF molecule of crystallization were put in geometrically calculated positions and those of the remaining two THF solvent molecules were ignored, it not being possible to distinguish between the oxygen and carbon atoms. Structure refinement was not straightforward because of the disorder involving the $Cu_4Cl_5^-$ anion. This consists of two parallel squares of copper atoms (Cu1A, Cu2A, Cu3A, and Cu4A, each one η^2-bonded to the terminal C–C bond of a pyrrole ring) and chlorine atoms (Cl3, Cl4, Cl5, and Cl6) stacked by 1.341(9) Å and rotated from each other by 45° (Figure 4 (bottom)). The Cu square is capped by a chlorine directed toward the cavity of the complex. This model could not be considered as satisfactory because of the presence in the ΔF map of four residual peaks significantly above the general background (2–6 e Å^{-3}) lying in the plane of the chlorines. They were interpreted as "partial" copper atoms, Cu1B, Cu2B, Cu3B, and Cu4B, each one diagonally coordinated to two chlorines. This model was successfully refined with the site occupation factors for the copper atoms given in Table 5, implying a statistical distribution of the Cu atoms consistent with the schemes given in Figure 5. The final difference map showed some residual peaks of about 1 e Å^{-3} in the region of the Cu_4Cl_5 anion and in the proximity of the cobalt atom. The accuracy of the present analysis is rather low owing to the Cu Kα radiation used to collect the intensity data which was the only one available at the time. Crystal decomposition prevented a subsequent data collection with the more suitable Mo Kα radiation.

Final atomic coordinates are listed in Tables 2–5 for non-H atoms and in supplementary Tables SII–SV for hydrogens. Thermal parameters are given in Tables SVI–SIX, bond distances and angles in Tables SX-SXII.[33]

Acknowledgment. We would like to thank the Fonds National Suisse de la Recherche Scientifique (Grant No. 20-33420-92) for financial support and Dr. Nazzareno Re, Università di Perugia (Italy), for magnetic calculations.

Supplementary Material Available: Tables giving crystal data and details of the structure determination, hydrogen atom coordinates, anisotropic and isotropic thermal parameters, bond lengths, and bond angles and figures showing ORTEP views of the $FeCl_4^{2-}$ anion in complex **4** (Figure S1) and of molecule B in complex **7** (Figure S2) (22 pages); listings of structure factors (43 pages). This material is contained in many libraries on microfiche, immediately follows this article in the microfilm version of the journal, and can be ordered from the ACS; see any current masthead page for ordering information.

(33) See paragraph at the end regarding supplementary material.